JOM, Vol. 74, No. 1, 2022
https://doi.org/10.1007/s11837-021-05015-z

Crystal Structure, Phase Stability, Microstructure, and Optical Properties of Transition Metal Incorporated Wide Band Gap Ga_2O_3

VISHAL ZADE ,[1,2,3] ROY SWADIPTA,[1] and C.V. RAMANA[1,2]

1.—Centre for Advanced Materials Research (CMR), University of Texas at El Paso, 500 W University Ave, El Paso, TX 79968, USA. 2.—Department of Mechanical Engineering, University of Texas at El Paso, 500 W University Ave, El Paso, TX 79968, USA. 3.—e-mail: vzade@miners.utep.edu

The effect of transition metal (TM) ion mixing on the crystal structure, surface morphology, microstructure, and optical properties of gallium oxide (Ga_2O_3) have been reported. The polycrystalline TM-mixed Ga_2O_3 (referred to TMGO; TM = Fe, Ti, W) materials were synthesized via a conventional, high-temperature solid-state chemical reaction method. The detailed investigation based on x-ray diffraction (XRD), scanning electron microscopy (SEM), and optical absorption measurements indicates the effect of Fe, Ti, and W incorporation on the structural and optical properties of Ga_2O_3. The marked difference in the mixing of various TM-ions (Fe^{3+}, Ti^{4+}, and W^{6+}) is strongly reflected in the solubility limit of the respective TM-ions. For the constant amount of TM-ion alloying/mixing, no secondary phase formation occurs with Fe or W, while TiO_2 secondary phase formation occurs for Ti. The optical band gap ($\sim$ 4.6 eV) of intrinsic Ga_2O_3 reduces significantly with Fe as compared to that of W and Ti.

INTRODUCTION

Gallium oxide (Ga_2O_3) is one of the family of wide band gap semiconductor oxides, and it has been attracting the scientific and engineering research community for the design and development of modern and novel optoelectronic and electronic devices.[1–10] The increased interest is attributed to the tunable properties exhibited by Ga_2O_3, which is quintessential for a range of applications, such as photocatalysis, optoelectronic, energy storage and conversion, and electronics.[1–15]

Gallium oxide (Ga_2O_3) exhibits polymorphism, which is subject to thermodynamic conditions of synthesis. This gives rise to an interesting, diverse crystal structure and properties for exploitation as a functional material in a variety of technological applications.[16–18] Exhaustive reports on the α, β, γ, δ, and ε phases of Ga_2O_3 are available in the literature.[12,16–22] Among these polymorphs, the β-Ga_2O_3 is known for its exceptional thermal and chemical stability at higher temperatures.[2,4,19,23,24] β-Ga_2O_3 has a wide band gap of $\sim$ 4.8 eV along with a high dielectric breakdown voltage of 8 MV cm^{-1}.[4,25–27] Like all oxides, β-Ga_2O_3 is considered for mixing with transition metals to derive tunable properties for various technological applications.

The claim for β-Ga_2O_3 as a technologically viable solution for a range of applications is substantiated by numerous experimental and theoretical efforts in recent years,[1,2,9,28–39] and is also influenced by the mixing and/or doping effects of β-Ga_2O_3. Silicon doping into β-Ga_2O_3 shows that there can be an overall control on the electrical conductivity.[32,40] Enhancement in n-type conductivity has been demonstrated with Si-doped β-Ga_2O_3 in comparison with the undoped β-Ga_2O_3, with the hypothesis of electron donor generation by Si^{4+} substitution on Ga sites.[32] Electrical properties such as carrier density and electrical resistivity are tuned by mixing Sn into β-Ga_2O_3.[41] An astute investigation deploying

(Received July 27, 2021; accepted October 28, 2021; published online November 29, 2021)

density function theory (DFT) provided critical insights regarding the change in electronic structure due to mixing and its subsequent implications on the properties of Ga_2O_3.[30,31] DFT calculations have predicted that W, Mo, and Re will act as deep donors and that Nb will behave as a shallow donor. Investigations into the behavior of dopants in thin films have been reported for β-Ga_2O_3.[9,34,35,37–39] The optical band gap β-Ga_2O_3 polycrystalline thin films show a decline with mixing elements, specifically with Cu,[9,34] Nb,[35] W,[38] and Ti,[39] with varying dopant concentrations and chemistry.[37,38,42]

The scope of this work extends to the study of Fe, Ti, and W, mixing them individually into β-Ga_2O_3 for a fundamental understanding of their structural properties. Our previous work has focused primarily on exploring the design and development of materials with controlled parameters. The change in properties was targeted towards the chemical, physical, structural, and optical[2,13,28,29,37–39,41–43] properties. As we continue to investigate the effects of TM mixing into β-Ga_2O_3, Fe-doped β-Ga_2O_3 via a solid-state synthesis route results in the Ga^{3+} substitution by Fe^{3+} in octahedral and tetrahedral positions due to its Shannon ionic radius proximity.[28] A detailed understanding of the dielectric properties, chemical composition, and crystal structure has been presented[36] along with other studies.[44,45] In conjunction, Ti-doped Ga_2O_3 ceramics were also synthesized by a high-temperature solid-state chemical reaction method which depicted a phase-pure compound for lower concentration of Ti dopant (< 5 at%).[41] As the concentration of Ti increases, an undissolved TiO_2 phase is observed.[28] Titanium mixing also showed abnormal grain growth and lattice twinning-induced striations which are unknown in intrinsic Ga_2O_3.[41] The effects of W-mixed Ga_2O_3 produced interesting results.[2] A lower W concentration resulted in a clear solid solution ($x \leq 0.10$), while a WO_3 secondary phase was observed in the structural characterization of W-doped Ga_2O_3 (GWO) at $x > 0.10$. Progressing from these results, it is important to compare and contrast the effect of various TM-ion mixing into Ga_2O_3, especially in the context of variable solubility limits of respective ions and expected changes in the electrical and optical properties. Hence, the importance of this study is to leverage the understanding of the mixing of TM-ions and its effects with respect to the surface/interface diffusion, which might be useful for hetero-structures and contacts. To keep this in focus, this work employed a simple and versatile solid-state chemical reaction method to study the structural properties in TM-GO compounds with varying TM content and chemistry.

MATERIALS AND METHODS

Synthesis

The transition metal-mixed Ga_2O_3 compounds [$(TM_xGa_{1-x})_2O_3$; referred to TMGO] were synthesized using a conventional solid-state reaction method. The concentration was kept at 0.1 at% due to the solubility limits and to avoid the formation of a secondary phase. Previously established procedures, methods, and processing conditions were adopted to synthesize the TM-doped Ga_2O_3 compounds in order to understand their electronic structure, crystal symmetry, and allied properties.[2,28,29,41,42] A detailed description for the individual TM-GO compound is described in the following sub-sections.

Iron (Fe)-Mixed Ga_2O_3

A detailed synthesis process for Fe-mixed Ga_2O_3 compounds has been described elsewhere.[28,42] The solid-state chemical reaction method requires a homogenous mixture of the precursors in stoichiometric proportions followed by calcination at 1100°C for a period of 6 h. The calcined powder was used to make pellets (8 mm diameter and 2 mm thickness) at an applied load of 5 ton for 60 s in a hydraulic press. These pellets were then sintered at 1200°C for 6 h to a better density.

Titanium (Ti)-Mixed Ga_2O_3

The synthesis of Ti-mixed Ga_2O_3 compounds has been described in detail elsewhere, which includes a solid-state, high-temperature chemical reaction method.[41] The charge balance is maintained by chemical composition calculations using $(TM_xGa_{1-x})_2O_3$. Using acetone as a wetting media, the precursors are finely ground in an agate mortar. This was followed by calcination at 1250°C for 12 h with intermediate grinding to relieve stresses in the ceramic powder. Poly vinyl alcohol (PVA) was added to ensure binding of the particles and to facilitate dispersion.[41] The final product was made using an MTI uniaxial hydraulic press at 1.5 ton and sintered at 1350°C for 8 h.[41]

Tungsten (W)-Mixed Ga_2O_3

The synthesis of W-mixed Ga_2O_3 compounds has been described in detail elsewhere.[2,29] The charge balance is maintained by chemical composition calculations using $(TM_xGa_{1-x})_2O_3$. The underlying process consists of forming a homogenous mixture of precursor WO_3 and Ga_2O_3 powders, followed by calcination at 1050°C for 12 h and then at 1150°C for 12 h. The PVA, which was used as a binding

agent, was added to the calcined powders before palletization. The obtained green pellets were sintered at 1250°C for 6 h keeping a temperature ramp-up of 5°C/min with a binder burnout at 500°C for 30 min.[2,29]

Methods

X-ray Diffraction (XRD)

The structural analysis was performed using a Rigaku Benchtop powder x-ray diffractometer (Mini Flex II). Scanning parameters were: 10°– 80° (2θ range), step size of 0.02° and scan rate of 0.6°/min.

Scanning Electron Microscopy (SEM)

The microstructural features reveal information about the samples after being subjected to temperature and other processing conditions. SEM (Hitachi – 4800) was used to obtain the micrographs of the TM-GO sample.

UV-visible–NIR Spectroscopy

Insights into elemental mixing can be obtained by understanding the optical absorption spectra which give additional information over x-ray diffraction analysis. The optical absorption spectra of the GWO sintered powders were collected using a UV–vis spectrophotometer (Lambda 1050; PerkinElmer).

RESULTS

Crystal Structure

The XRD data of TM-GO ceramics are shown in Fig. 1. For comparaision, the XRD pattern of intrinsic Ga_2O_3 is also presented. For Fe mixing, there is no discernible difference between intrinsic Ga_2O_3 and Fe-mixed Ga_2O_3 compounds. The XRD patterns clearly indicate that the intrinsic Ga_2O_3 and Fe-mixed Ga_2O_3 compounds crystallize in monoclinic phase with the C2/m space group (JCPDS #00-041-1103).[31] Furthermore, the XRD patterns confirm the phase purity of the Fe-mixed Ga_2O_3 compounds, in which there is no sign of a secondary phase.

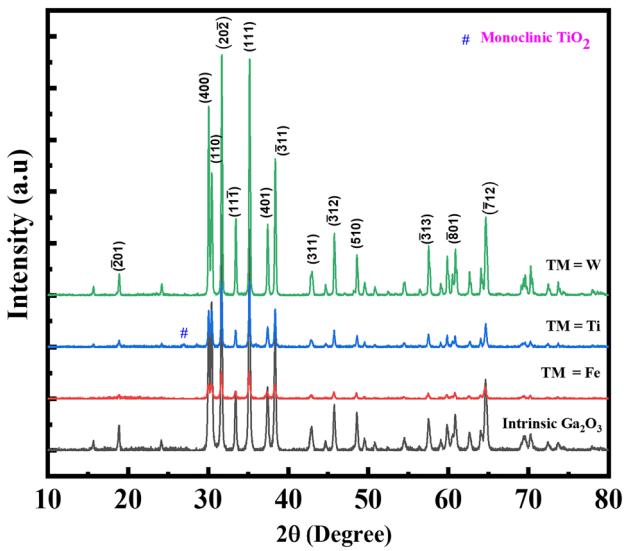

Fig. 1. XRD patterns of TM-GO compounds. Comparative XRD data of intrinsic and TM-ion mixed Ga_2O_3 compounds clearly indicate the crystal structure differences as a function of TM-ions.

From the XRD pattern shown in Fig. 1, it is clearly evident that there is a secondary TiO_2 phase formation. While the single-phase Ti-Ga_2O_3 compound formation is predominant, the peaks due to TiO_2 secondary phase formation appear only with a minor intensity. Perhaps the secondary phase may be due to unreacted TiO_2 rutile phase.

Tungsten mixing is somewhere in between the Ti and Fe. However, the XRD data clearly indicate that, for W mixing, single-phase compound formation occurs. The unit cell dimensions are, however, slightly reduced compared to intrinsic Ga_2O_3. Perhaps the smaller ionic radius of W^{6+} compared to Ga^{3+} might be the reason for the reduction in the unit cell dimensions, i.e., shrinkage in unit cell volume upon W ion incorporation into Ga oxide. Furthermore, the peak shift magnitude is not uniform for different diffraction planes, as seen in the XRD data. While the optimum conditions were employed in this work, as reported previously, the XRD patterns of GWO calcined at lower temperatures (1050°C) clearly reveal insolubility of WO_3 even at lower (x = 0.1) concentrations.[2] The insolubility of WO_3 in Ga_2O_3 is attributed to two factors.[2]

Morphology and Microstructure

The comparative SEM micrographs as shown in Fig. 2 for TM-GO compounds provide insights into the effect of TM mixing on the surface morphology and microstructure of Ga_2O_3. The SEM data of intrinsic Ga_2O_3 illustrate a rod-shaped grain morphology, which is a characteristic feature of pure Ga oxide ceramics.[2,34] The rod-shaped grains further characterize the morphology of intrinsic Ga_2O_3 with a size varying from approximately 0.5 μm to 2.0 μm (width) and 1.0 μm to 4.0 μm (length). Iron mixing shows a mild change in the microstructure, as the shape change indicates in the SEM data (Fig. 3). The particles coalesce with Fe inclusion, which is the characteristic feature with a reduction in size with increasing Fe content from 3.5 μm to $\sim$ 2.0 μm. Along with the fine-grain size distribution, a smooth and uniform distribution can also be observed. The microstructure and morphology of GFO compounds directly correlates with the observation, based on the XRD and XANES studies, that the doped Fe preferentially occupies sites in the parental Ga sites by forming substitutional solid solutions and maintains the same crystal symmetry as that of the intrinsic Ga_2O_3.[28]

Interestingly, W incorporation into Ga_2O_3 shows a significant change in the morphology even with a smaller addition of W mixing. The grains initially

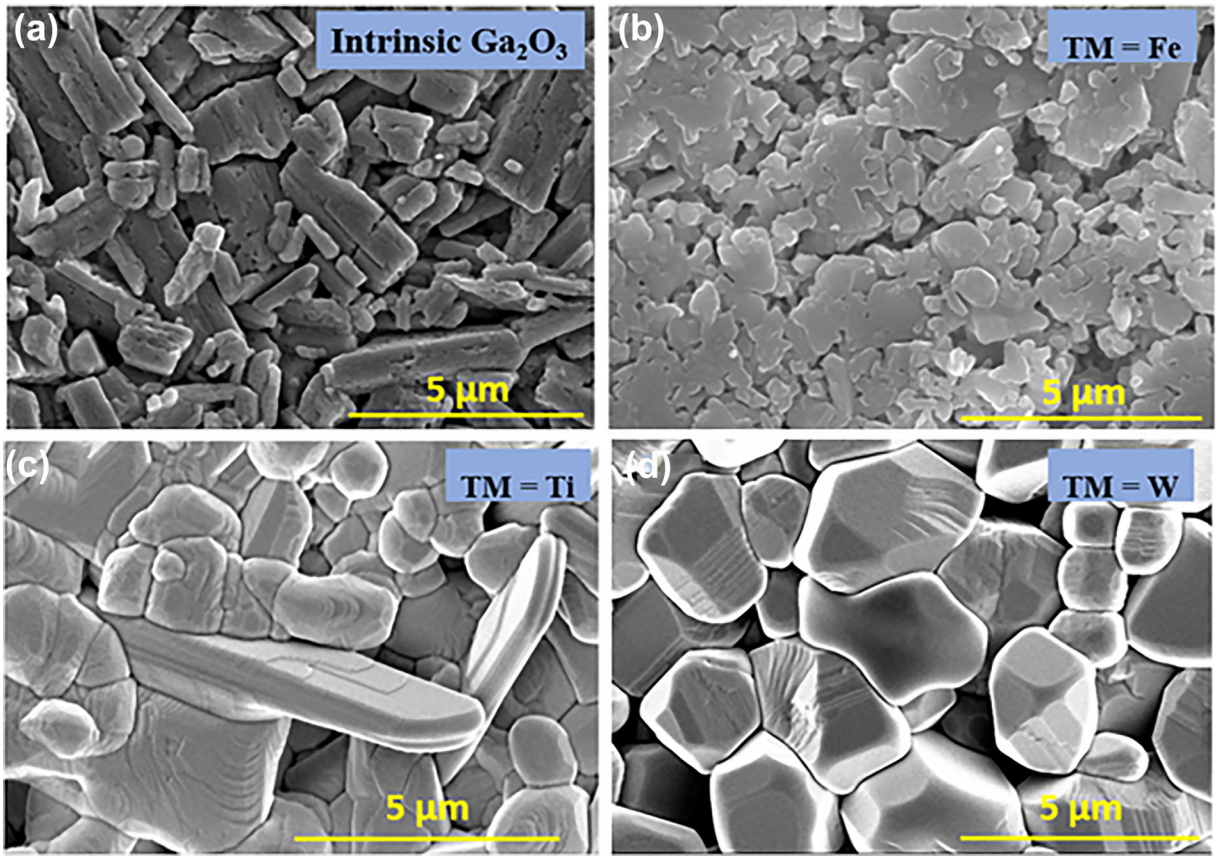

Fig. 2. SEM micrographs of TMGO compounds. The effect of TM ions on the morphology and microstructure is evident.

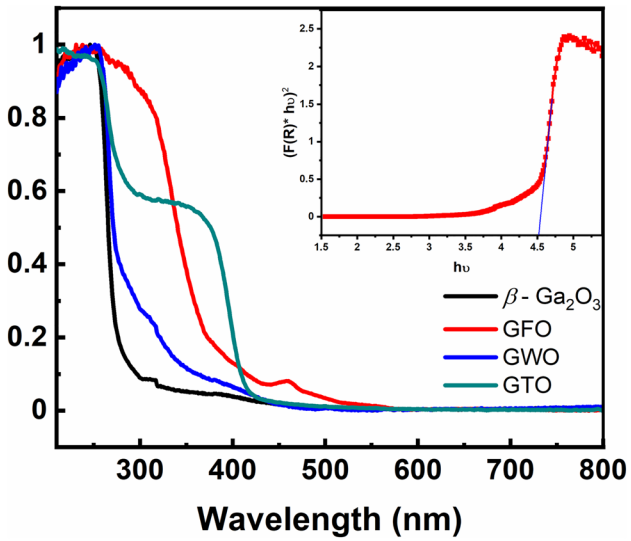

Fig. 3. Optical absorption spectra of TMGO compounds. Inset the illustrative case of W mixed Ga_2O_3.

show a spherical nature, and then become more faceted in either square or hexagonal geometry. Similar to W mixing, the Ti mixing also drastically changes the morphology of Ga_2O_3. The rod-like shaped morphology of intrinsic Ga_2O_3 changes to a nearly spherical grain morphology with Ti mixing. Also, abnormal grain growth can be noted in Ti-doped Ga_2O_3 compounds.

Optical Properties

The optical absorption data of TMGO compounds are presented and compared in Fig. 3. The absorption spectrum indicate an absorption edge at ≈ 280 nm in the UV region. These characteristic features of intrinsic Ga_2O_3 are in good agreement with those reported in the literature.

It is important to note that the red shift observed in the optical absorption edge in GWO ceramic compounds has also been reported for W-doped Ga_2O_3 polycrystalline thin films.[37] The observed shift in these W-mixed Ga oxide ceramics is substantially higher compared to that reported for GWO thin films.[29] It can be seen that the optical absorption edge experiences a substantial red shift with Fe-mixed Ga oxide compounds. Also, in addition to the red shift in the fundamental absorption edge, the features of the optical absorption edge are slightly different for the case of Ti into Ga_2O_3. The formation of a secondary TiO_2 phase may be the reason for such a change or additional features in the absorption spectrum.

The optical absorption data were further analyzed to quantify the band gap reduction. For this purpose, the Tauc method was used, which is quite

routinely employed in the optical band gap determination of semiconductors and insulators.[46,47] The Tauc relationship is given by:

$$\alpha h\upsilon = A\left(h\upsilon - E_g\right)^n \quad (1)$$

where α is an absorption coefficient, $h\upsilon$ the incident photon energy, A proportionality constant, E_g the band gap, and n an index determining the electronic transitions type (n takes values of ½ for direct allowed transition, 2 for indirect allowed transition, 3/2 for direct forbidden transition, and 3 for indirect forbidden transition).[2] The Kubelka–Munk function [$F(R)$] is equivalent to the reflectance/absorption spectra absorbance in any UV-vis experiment.[48–50] The Kubelka–Munk function relationship is given as:[51]

$$F(R) = \frac{(1-R)^2}{2R} = \frac{K}{S} \quad (2)$$

where R is the reflectance, K the absorption coefficient, and S a scattering factor.

For clarity purposes, the representative Tauc plot of GWO is shown in the inset of Fig. 3. β-Ga_2O_3 exhibiting both direct and indirect band gaps has been evidenced by theoretical and experimental work.[52] The results have also shown that the indirect band gap is lower than the direct band gap.[52] The hybrid density functional theory reports the direct and indirect band gap values at 4.88 eV and 4.84 eV, respectively,[23] while experimentally determined direct and indirect band gaps in β-Ga_2O_3 single crystals are 4.48 eV and 4.43 eV, respectively.[53] A small energy differences of 0.04 eV in the theoretical findings and 0.05 eV in the experimental findings were noticed for direct and indirect band transitions. The present study reports a direct band gap of 4.60 eV for intrinsic β-Ga_2O_3. The lower value of the band gap for Ga_2O_3 bulk ceramics as compared to the reported values for single crystals can be associated with (1) high-temperature processing (solid-state reaction method) induced lattice strain[54] and (2) relatively higher point defects in bulk ceramics than in single crystals. The variation in band gap with TM-ions is shown in Fig. 4. The trend suggests electronic structure changes in TMGO compounds compared to intrinsic Ga_2O_3.

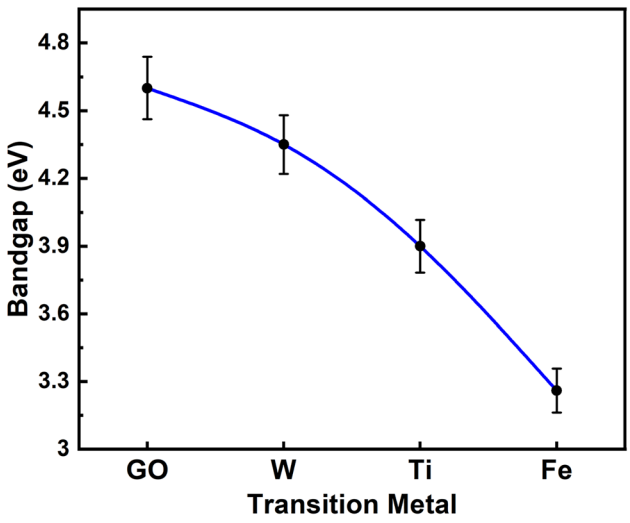

Fig. 4. Band gap variation in TMGO compounds.

Table I. Ionic radii of Fe, Ti, and W ions with respect to Ga ions in Ga_2O_3

Atom	Valence	Ionic radii
Ga	3+	0.47 Å (IV), 0.62 Å (VI)
Fe	3+	0.49 Å (IV) high spin 0.55 Å (VI) low spin 0.645 Å (VI) high spin
Ti	4+	0.42 Å (IV), 0.605 Å (VI)
W	6+	0.42 Å (IV), 0.60 Å (VI)

IV coordinate (tetrahedral), *VI* coordinate (octahedral).

DISCUSSION

The chemical valence states and ionic radii of Fe, Ti, and W with respect to Ga are presented in Table I. The ionic radii of Ga and Fe are very close; therefore, in GFO compounds, Fe does not form any intrinsic defect by itself along with isovalent electron configuration. However, the scenario is fully different for the case of Ti mixing in Ga_2O_3. The XRD results indicate that the Ti mixing results in the formation of a TiO_2 secondary phase in addition to the single-phase Ti-Ga_2O_3 compound. Note that the Shannon ionic radii of Ti^{4+} also closely match with those of Ga^{3+} in both tetrahedral and octahedral coordinations.[55] Additionally, the formation energies of their respective oxides, i.e., TiO_2 and Ga_2O_3, are also similar.[56] The formation enthalpy of TiO_2 is – 10.18 eV (Ti-rich condition), which closely matches that of Ga_2O_3 (– 10.73eV).[30] Hence, the difference in formation enthalpies can be ruled out for the observed insolubility and TiO_2 formation. Moreover, the electronegativity values of Ti^{4+} [1.5] and Ga^{3+} [1.8] are in close proximity. Therefore, the aliovalent characteristics of Ti^{4+} and Ga^{3+} would be a possible reason for the insolubility of Ti, leading to the formation of a secondary phase (TiO_2). The formation of a TiO_2 secondary phase was also observed in sputter-deposited nanocrystalline Ga-Ti-O films where the films were co-deposited using

Ti metal and Ga_2O_3 targets. Thus, the formation of TiO_2 for Ti-mixed or -doped Ga_2O_3 compounds both in polycrystalline ceramics and thin film materials seems to originate by means of chemically driven processes.

For the present case of Ti-mixed Ga_2O_3 compounds, the volume fraction of the secondary TiO_2 phase was calculated using the intensity of XRD reflections of rutile TiO_2 (110) and Ga_2O_3 (111) using the Eq. (7):[57,58]

$$\text{Volume fraction of } TiO_2 \text{ phase} = \frac{I_{TiO_2(110)}}{\left(I_{Ga_2O_3(111)} + I_{TiO_2(110)}\right)} \quad (3)$$

The estimated volume fraction of the TiO_2 phase in the GTO compound is only 4%. However, such a minor component of the secondary phase of the foreign TM-ion is more than sufficient to induce strain in the lattice of the intrinsic material. It can be hypothesized that, due to the smaller ionic radii of Ti^{4+} as compared to Ga^{3+}, it should lead to a shift in the Bragg position towards a higher Bragg angle. This anomaly can be attributed to the Ti-induced local structural disorder resulting from a global charge imbalance.

For W mixing, the structural data indicate that the resulting GWO compounds are almost similar to intrinsic Ga_2O_3. However, the effect of ionic size was evident. The relatively smaller ionic radius of W^{6+} ions compared to Ga^{3+} ions may contribute to the unit cell size reduction. This could be the reason why a shift was observed in the XRD peaks towards the higher diffraction angle.

Similar to the case of Ti, in order to derive a comprehensive understanding and quantification of solubility limits, the volume fraction of unreacted WO_3 phase is calculated using:

$$\text{Volume fraction of unreacted } WO_3 = \frac{I_{(112)}WO_3}{I_{(111)}Ga_2O_3 + I_{(112)}WO_3} \times 100 \quad (4)$$

The amount of unreacted WO_3 in GWO is extremely small (< 2%). Although the ionic radii of W^{6+} and Ga^{3+} are in close proximity, the formation energy of W^{6+} in the Ga_2O_3 lattice dictates the solubility limit of W. To further elaborate, the concentration of doping in a given compound is determined by the formation energy of a specific defect or impurity at the parent lattice site.[2,30,31]

Moving on to the optical properties, the band gap of intrinsic Ga_2O_3 is 4.56 (± 0.01) eV, which is in good agreement with that reported in the literature.[23,53] A large shift in the band gap occurs with Fe incorporation into Ga_2O_3. The GFO compounds experience a significant reduction in band gap from 4.56 eV to 3.34 eV, while the shift induced by the W and Ti ions falls in between the range. While such a reduction in band gap is also noted in Cu-, W-, Mo-, and Ti-doped Ga_2O_3,[34,36,59,60] the red shift observed in the Fe-incorporated Ga_2O_3 compounds is significant, and this enhanced narrowing of the band gap occurring even for a relatively lower content of Fe is very significant. The ionic radii of Ga and Fe are in excellent close match with each other; Ga^{3+} of 0.62 Å (octahedral coordination) and 0.47 Å (tetrahedral coordination), and Fe^{3+} of 0.64 Å (octahedral coordination) and 0.49 Å (tetrahedral coordination). Therefore, Fe^{3+}can be substituted in the Ga site, which can replace Ga^{3+} from both the octahedral and tetrahedral positions in stoichiometric proportion. Thus, no perturbation to the parent crystal structure, i.e., monoclinic structure of β-Ga_2O_3, is seen. Under such isostructural configurations, electronic structure changes occur due to the Fe substituting for Ga. Thus, the substantial red shift observed in the band gap can be explained based on the *sp-d* exchange interaction (see Fig. 5) between the valance band electrons and the localized *d* electrons of Fe in Ga_2O_3. The *sp-d* exchange interactions lead to positive and negative corrections to the valance and conduction bands, and, as a consequence, band gap narrowing occurs in the systems with *sp-d* exchange interactions. In the present case, the outermost electron configurations of Ga^{3+} and Fe^{3+} are $3d^{10}$ and $3d^5$, respectively. Therefore, in intrinsic Ga_2O_3, 3d electrons are not involved in hybridization, whereas in the case of Fe-mixed Ga_2O_3 compounds, $3d^5$ electrons are involved in hybridization with O p-orbitals. Owing to this, there are strong *s-d* and *p-d* exchange interactions present in GFO compounds which lead to abrupt band gap narrowing. These interactions, and, hence, the spectral selectivity and band gap, can be tuned by carefully controlling the Fe content and, hence, the chemistry in GFO compounds.

Figure 5 displays schematic energy diagram of intrinsic β-Ga_2O_3 and Fe^{3+}-doped Ga_2O_3, and clearly shows positive and negative corrections to the valance and conduction bands due to sp-d exchange interactions in Fe^{3+} in the Ga_2O_3,-associated band gap narrowing. As explained, in the case of intrinsic β-Ga_2O_3, the valance band edge is dominated by O-2p orbitals and the conduction band is dominated by Ga-4s orbitals, whereas in the case of Fe^{3+}-doped compounds, the valance band edge is dominated by O-2p orbitals and the conduction band edge is dominated by Ga-4s and Fe-3d, in contrast to intrinsic Ga_2O_3. The sp-d exchange originates in Fe-doped compounds due to the contribution of Fe-3d electrons to the conduction band.

The proposed hybridization and exchange interactions will also account for the observed band gap reduction in other TMGO compounds. For the case of W, the band gap reduction noted in GWO compounds is also due to *sp-d* exchange interactions, arising from the localized electrons of W 5*d* orbitals. In pure Ga_2O_3, the contribution of O *p* orbitals to the valance and conduction bands is predominantly due to the Ga *4s* character, whereas in W-mixed Ga_2O_3-doped compounds, the

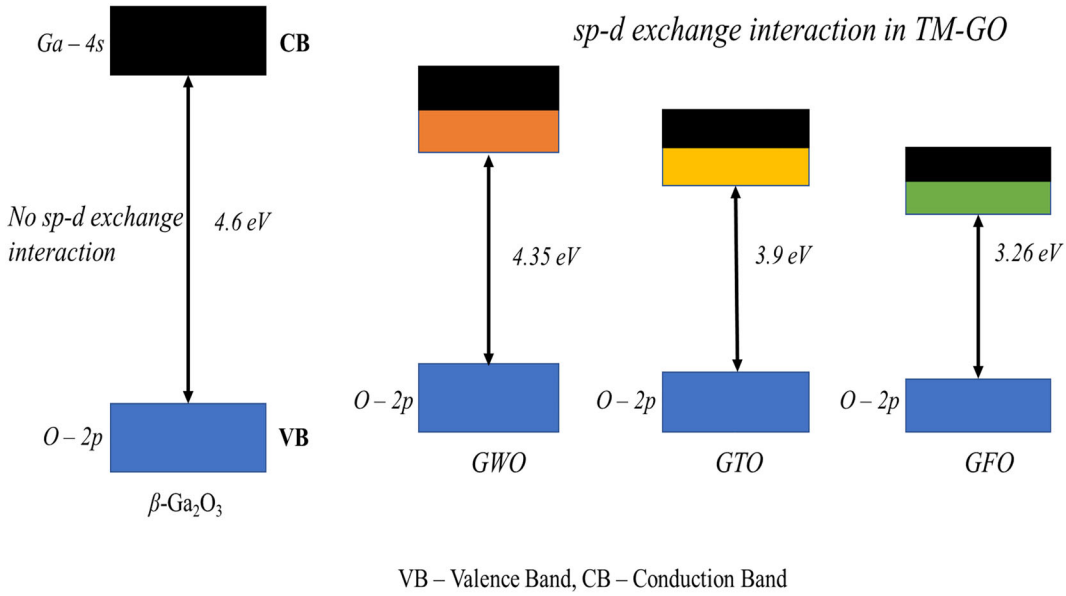

Fig. 5. Schematic energy diagram of intrinsic Ga_2O_3 and TM-GO compounds.

conduction band is dominated by W *5d* along with the Ga *4s* character. Hence, the contribution of W 5*d* orbitals to the conduction band leads to *sp-d* exchange interactions between the valance band delocalized electrons (O *s* and *p* orbitals) and the conduction band localized electrons (*W 5d* orbitals) in GWO compounds. The *sp-d* exchange interactions make positive and negative corrections to the valance band and the conduction band, respectively, which results in band narrowing of GWO compounds, as indicated in Fig. 5.

CONCLUSION

Transition metal mixed Ga_2O_3 materials were synthesized via a conventional, high-temperature solid-state chemical reaction method. The TM mixing-induced effects are fully reflected on the crystal structure, surface morphology, microstructure, and optical properties. Iron mixing into Ga_2O_3 proceeds with the formation of a phase-pure solid solution, where there is no discernible difference between intrinsic Ga_2O_3 and Fe-mixed Ga_2O_3 materials, as evidenced in the XRD data and analyses. On the other hand, for Ti mixing, TiO_2 secondary phase formation occurs. However, the amount of TiO_2 secondary phase is very low. The TM mixing and compound formation reduces the band gap of intrinsic Ga_2O_3. The band gap of intrinsic, polycrystalline Ga_2O_3 ceramic was $\sim$ 4.60 eV, which reduces to 3.26 eV for Fe-mixed Ga_2O_3 compounds. The band gap reduction is more with Fe compared to that of W and Ti mixing into Ga_2O_3. The observed band gap reduction in TM-GO compounds is explained on the basis of the *sp-d* exchange interactions, which lead to positive and negative corrections to the valance and conduction bands. Compared to intrinsic Ga_2O_3, where the O *p* orbitals contribute to the valance band while the conduction band is predominantly due to the Ga *4s* character, the TM-GO compounds experience the hybridization and contribution from TM *d*-orbitals leading to *sp-d* exchange interactions between the valance band delocalized electrons (O *s* and *p* orbitals) and the conduction band localized electrons. The scientific understanding of the crystal structure, phase stability, microstructure, and optical properties of TM-GO compounds, and the demonstrated approach to derive the tunable optical properties, may be useful while considering such materials for practical optoelectronic and energy-related applications.

ACKNOWLEDGEMENTS

The authors acknowledge, with pleasure, support from the National Science Foundation (NSF) with NSF-PREM Grant #DMR-1827745.

CONFLICT OF INTEREST

On behalf of all authors, the corresponding author states that there is no conflict of interest.

REFERENCES

1. G. Sinha and A. Patra, *Chem. Phys. Lett.* 473, 151 (2009).
2. V. Zade, B. Mallesham, S. Shantha-Kumar, A. Bronson, and C.V. Ramana, *Inorg. Chem.* 58, 3707 (2019).
3. M. Higashiwaki, and G.H. Jessen, *Appl. Phys. Lett.* 112, 060401 (2018).
4. S.J. Pearton, J. Yang, P.H. CaryIV, F. Ren, J. Kim, M.J. Tadjer, and M.A. Mastro, *Appl. Phys. Rev.* 5, 011301 (2018).
5. S.B. Patil, I.Y. Kim, J.L. Gunjakar, S.M. Oh, T. Eom, H. Kim, S.-J. Hwang, and A.C.S. App, *Mater. Interfaces* 7, 18679 (2015).
6. Y. Usui, D. Nakauchi, N. Kawano, G. Okada, N. Kawaguchi, and T. Yanagida, *J. Phys. Chem. Solids* 117, 36 (2018).
7. M. Ogita, K. Higo, Y. Nakanishi, and Y. Hatanaka, *Appl. Surf. Sci.* 175, 721 (2001).

8. S. Ghose, S. Rahman, L. Hong, J.S. Rojas-Ramirez, H. Jin, K. Park, and R. Klie, *J. Appl. Phys.* 122, 095302 (2017).
9. S.E. Choi, Y.T. Oh, H.K. Ham, T.W. Kim, G.S. Heo, J.W. Park, B.H. Choi, and D.C. Shin, *Curr. Appl. Phys.* 11, S255 (2011).
10. X. Wang, F. Zhang, K. Saito, T. Tanaka, M. Nishio, and Q. Guo, *J. Phys. Chem. Solids* 75, 1201 (2014).
11. C. Ramana, Properties of sputter-deposited gallium oxide, in: *Gallium Oxide*, (Amersterdam: Elsevier, 2019) p 47.
12. H. He, R. Orlando, M.A. Blanco, R. Pandey, E. Amzallag, I. Baraille, and M. Rérat, *Phys. Rev. B* 74, 195123 (2006).
13. S.S. Kumar, E.J. Rubio, M. Noor-A-Alam, G. Martinez, S. Manandhar, V. Shutthanandan, S. Thevuthasan, and C.V. Ramana, *J. Phys. Chem. C* 117, 4194 (2013).
14. W. Zhang, B.S. Naidu, J.Z. Ou, A.P. O'Mullane, A.F. Chrimes, B.J. Carey, Y. Wang, S.-Y. Tang, V. Sivan, A. Mitchell, and A.C.S. Appl, *Mater. Interfaces* 7, 1943 (2015).
15. J. Liu and G.K. Zhang, *Mater. Res. Bull.* 68, 254 (2015).
16. H. Sun, K.-H. Li, C.T. Castanedo, S. Okur, G.S. Tompa, T. Salagaj, S. Lopatin, A. Genovese, and X. Li, *Cryst. Growth Des.* 18, 2370 (2018).
17. Y. Chen, X. Xia, H. Liang, Q. Abbas, Y. Liu, and G. Du, *Cryst. Growth Des.* 18, 1147 (2018).
18. S. Yoshioka, H. Hayashi, A. Kuwabara, F. Oba, K. Matsunaga, and I. Tanaka, *J. Phys. Condens. Matter* 19, 346211 (2007).
19. J. Åhman, G. Svensson, and J. Albertsson, *Acta Crystallogr. Sect. C* 52, 1336 (1996).
20. M. Bartic, C.-I. Baban, H. Suzuki, M. Ogita, and M. Isai, *J. Am. Ceram. Soc.* 90, 2879 (2007).
21. H.Y. Playford, A.C. Hannon, E.R. Barney, and R.I. Walton, *Chem. Eur. J.* 19, 2803 (2013).
22. J.E. Swallow, C. Vorwerk, P. Mazzolini, P. Vogt, O. Bierwagen, A. Karg, M. Eickhoff, J. Schörmann, M.R. Wagner, and J.W. Roberts, Influence of Polymorphism on the Electronic Structure of Ga2O3, *arXiv* preprint arXiv: 2005.13395 (2020).
23. H. Peelaers and C.G. Van de Walle, *Phys. Status Solidi (B)* 252, 828 (2015).
24. H.J. Lin, J.P. Baltrus, H.Y. Gao, Y. Ding, C.Y. Nam, P. Ohodnicki, P.X. Gao, and A.C.S. Appl, *Mater. Interfaces* 8, 8880 (2016).
25. G. Yang, S. Jang, F. Ren, S.J. Pearton, J. Kim, and I.C.S. Appl, *Mater. Interfaces* 9, 40471 (2017).
26. Y. Yao, R.F. Davis, and L.M. Porter, *J. Electron. Mater.* 46, 2053 (2017).
27. M. Higashiwaki, K. Sasaki, A. Kuramata, T. Masui, and S. Yamakoshi, *Phys. Status Solidi (A)* 211, 21 (2014).
28. S. Roy, B. Mallesham, V.B. Zade, A. Martinez, V. Shutthanandan, S. Thevuthasan, and C.V. Ramana, *J. Phys. Chem. C* 122, 27597 (2018).
29. V. Zade, B. Mallesham, S. Roy, V. Shutthanandan, and C. Ramana, *ECS J. Solid State Sci. Technol.* 8, Q3111 (2019).
30. H. Peelaers and C. Van de Walle, *Phys. Rev. B* 94, 195203 (2016).
31. C. Tang, J. Sun, N. Lin, Z. Jia, W. Mu, X. Tao, and X. Zhao, *RSC Adv.* 6, 78322 (2016).
32. E.G. Víllora, K. Shimamura, Y. Yoshikawa, K. Aoki, and N. Ichinose, *J. Cryst. Growth* 270, 420 (2004).
33. X. Wang, S. Shen, S. Jin, J. Yang, M. Li, X. Wang, H. Han, and C. Li, *PCCP* 15, 19380 (2013).
34. Y. Zhang, J. Yan, Q. Li, C. Qu, L. Zhang, and W. Xie, *Mater. Sci. Eng. B* 176, 846 (2011).
35. H. Zhang, J. Deng, P. Duan, R. Li, Z. Pan, Z. Bai, L. Kong, and J. Wang, *Vacuum* 155, 465 (2018).
36. A.A. Dakhel, *J. Mater. Sci.* 47, 3034 (2012).
37. E. Rubio, T. Mates, S. Manandhar, M. Nandasiri, V. Shutthanandan, and C. Ramana, *J. Phys. Chem. C* 120, 26720 (2016).
38. E.J. Rubio and C.V. Ramana, *Appl. Phys. Lett.* 102, 191913 (2013).
39. S. Manandhar, A.K. Battu, S. Tan, R. Panat, V. Shutthanandan, and C. Ramana, *J. Mater. Sci.* 54, 11526 (2019).
40. Y. Zhang, G. He, W. Wang, B. Yang, C. Zhang, and Y. Xia, *J. Mater. Sci. Tech.* https://doi.org/10.1016/j.jmst.2020.03.007 (2020).
41. M. Bandi, V. Zade, S. Roy, A.N. Nair, S. Seacat, S. Sreenivasan, V. Shutthanandan, C.G. Van de Walle, H. Peelaers, and C.V. Ramana, *Cryst. Growth Des.* 20, 1422 (2020).
42. B. Mallesham, S. Roy, S. Bose, A.N. Nair, S. Sreenivasan, V. Shutthanandan, and C.V. Ramana, *ACS Omega* 5, 104 (2020).
43. J.F. Moulder, *Handbook of x-ray Photoelectron Spectroscopy* (Eden Prairie, Perkin-Elmer, 1995).
44. W. Li, S.Y. Qiu, N. Chen, and G.P. Du, *J. Mater. Sci. Tech.* 26, 682 (2010).
45. Y. Zhang, G. He, W. Wang, B. Yang, C. Zhang, and Y. Xia, *J. Mater. Sci. Tech.* 50, 1 (2020).
46. J. Tauc, *Mater. Res. Bull.* 3, 37 (1968).
47. J. Tauc, R. Grigorovici, and A. Vancu, *Phys. Status Solidi (B)* 15, 627 (1966).
48. I. Ganesh, P.P. Kumar, A.K. Gupta, P.S. Sekhar, K. Radha, G. Padmanabham, and G. Sundararajan, *Process App. Ceram.* 6, 21 (2012).
49. H.D.S. Oliveira, A.C. Silva, J.P. de Mesquita, F.V. Pereira, D.Q. Lima, J.D. Fabris, F.C. Moura, and L.C. Oliveira, *New J. Chem.* 37, 2486 (2013).
50. A.H. Reshak, Z. Alahmed, J. Bila, V.V. Atuchin, B.G. Bazarov, O.D. Chimitova, M.S. Molokeev, I.P. Prosvirin, and A.P. Yelisseyev, *J. Phys. Chem. C* 120, 10559 (2016).
51. B. Nandan, B. Venugopal, S. Amirthapandian, B. Panigrahi, and P. Thangadurai, *J. Nanopart. Res.* 15, 1999 (2013).
52. K.A. Mengle, G. Shi, D. Bayerl, and E. Kioupakis, *Appl. Phys. Lett.* 109, 212104 (2016).
53. T. Onuma, S. Saito, K. Sasaki, T. Masui, T. Yamaguchi, T. Honda, and M. Higashiwaki, *Jpn. J. Appl. Phys.* 54, 112601 (2015).
54. S. Santhosh, M. Mathankumar, S. Selva Chandrasekaran, A. Nanda Kumar, P. Murugan, and B. Subramanian, *Langmuir* 33, 19 (2016).
55. R.D. Shannon, *Acta Crystallogr. Sect. A* 32, 751 (1976).
56. H. Zhu, P. Zhou, X. Li, and J.-M. Liu, *Phys. Lett. A* 378, 2719 (2014).
57. A.O. Juma, E.A.A. Arbab, C.M. Muiva, L.M. Lepodise, and G.T. Mola, *J. Alloys Compd.* 723, 866 (2017).
58. D. Singh, B. Mallesham, A. Deshinge, K. Joshi, R. Ranjith, and V. Balakrishnan, *Mater. Res. Express* 5, 116303 (2018).
59. A.K. Battu, S. Manandhar, and C.V. Ramana, *Mater. Today Nano* 2, 7 (2018).
60. A.K. Battu, S. Manandhar, V. Shutthanandan, and C. Ramana, *Chem. Phys. Lett.* 684, 363 (2017).